Available online at https://link.springer.com/journal/42241
http://www.jhydrodynamics.com
Journal of Hydrodynamics, 2021, 33(3): 503-509
https://doi.org/10.1007/s42241-021-0055-3

Vortex tuning of a submarine by Liutex force field model *

Liu-shuai Cao[1], Song-tao Chen[1], De-cheng Wan[1, 2], Yi-qian Wang[3]
1. *Computational Marine Hydrodynamics Lab (CMHL), School of Naval Architecture, Ocean and Civil Engineering, Shanghai Jiao Tong University, Shanghai 200240, China*
2. *Ocean College, Zhejiang University, Zhoushan 316021, China*
3. *School of Mathematical Science, Soochow University, Suzhou 215006, China*

(Received May 7, 2021, Revised June 8, 2021, Accepted June 9, 2021, Published online July 5, 2021)

Abstract: Vortical structures of a submarine with appendages are fully turbulent and complex. Thus, flow control and vortex manipulation are of great importance for the hydrodynamic performance and acoustic characteristics. Take the generic submarine model DARPA Suboff as the test case, a vortex tuning method based on the Liutex force field is proposed to manipulate the vorticity field. Viscous flow past the submarine model in straight-line motion at a Reynolds number of 1.2×10^7 is achieved by solving the Reynolds averaged Navier-Stokes (RANS) equations. Multi-block structured mesh topology is used to discretize the computational domain, and the shear stress transport (SST) k-ω turbulence model is implemented to close the equations. The control of vortex is achieved by introducing additional source terms based on Liutex vortex definition and identification system to the RANS equations. The resistance acting on the submarine, flow field as well as the vortical structures are compared and analyzed. Results show that Liutex force model can effectively reduce the resistance by 9.31% and change the vortical structures apparently.

Key words: Vortex tuning, vortical structures, submarine, vortex identification, Liutex force field model

Introduction

Vortical structures and wakes of a submarine play an important role for the hydrodynamic performance and acoustic characteristics. Due to the complexity of fully appended submarine geometry, which typically consists of a main body hull, a sail, and several control surfaces (or fins), the wakes feature a wealth of coherent structures and anisotropic turbulence. Even in steady motion at a constant depth, there exist junction or "horseshoe" vortices originating at the intersection of the control surfaces (including the sail) and the hull, tip vortices are generated at the outboard extent of the control surfaces[1]. Further, when the submarine undergoes maneuvering motions, there are many additional sources of longitudinal vorticity[2]. A complex, three-dimensional separation can occur over the body which generates strong streamwise vortices that are discharged into the wakes. These vortices produce forces and moments acting on the submarine body that can lead to undesirable motions.

Since the 1980s, with the development of fluid experimental technology and numerical computation method, the flow measurement, numerical simulation, and optimization of control on detailed flow structures around the submarine have become important parts in submarine hydrodynamics. Many researches have been devoted to the vortical structures[3], wakes[4-5], and hydrodynamic loads[6] of bare hull[7] and fully appended submarine[8] in straight-line[9], oblique[10], rotating[11] and maneuvering[12] motions.

To improve the stealth and power performance of the submarine, people have long been desiring to find useful methods to control the submarine wakes and vortices. In this regard, several methods for controlling the horseshoe vortex have been presented. Liu et al.[13] proposed a new method to control the horseshoe vortex by vortex control baffler. The detached eddy simulation (DES) results showed that a kind of attached vortex with rotation direction opposite to horseshoe vortex, was generated by the vortex control baffler, and the strength of the horseshoe vortex was significantly reduced. After that, in order to weaken the horseshoe vortex, Liu et al.[14] designed vortex

* Projects supported by the National Natural Science Foundation of China (Grant Nos. 52001210, 51879159), the National Key Research and Development Program of China (Grant Nos. 2019YFB1704200, 2019YFC0312400).
Biography: Liu-shuai Cao (1990-), Male, Ph. D., Assistant Professor, E-mail: liushuaicao@sjtu.edu.cn
Corresponding author: De-cheng Wan, E-mail: dcwan@sjtu.edu.cn

control bafflers adapted for the fully appended DARPA Suboff model. Then, unsteady forces of three kinds of propellers were calculated numerically. The results showed that the amplitudes of the unsteady forces acting on the blades of all three propellers decreased by 50% to 80% due to the effects of the vortex control baffler. Later, they developed a modified method to break the vortex core by a vortex baffle[15]. Numerical simulations showed that, with the breakdown of the vortex core, many unstable vortices were shed and the energy of the horseshoe vortex dissipated quickly, so that the uniformity of the submarine wakes was improved. This method could improve the wake uniformity in cases of high Reynolds numbers (Re) as well, and had no adverse effects on the maneuverability and the speed ability of the submarine.

Liu et al.[16] investigated a noise suppression mechanism by putting leading-edge serrations on the sail hull of the DARPA Suboff model. They found that the cone shape of leading-edge serrations can decrease the intensity of the adverse pressure gradient and produce counter-rotation vortices, which would destroy the formation of the horseshoe vortex and delay the tail vortex. At least 6 decibel reduction of hydrodynamic noise was achieved. Saeidinezhad et al.[17] made use of oil smoke flow visualization techniques to explore and describe complicated flow patterns over the axisymmetric body considering two different nose shapes. Results indicated that the nose curvature had great influence on the vortical flow structure and separation reattachment locations. Manshadi et al.[18] investigated ways to reduce separated flow by using vortex generators. Numerical simulations showed that the strength of the separation was significantly reduced for the model with the vortex generators. The results showed that the vortex generators placed along the submarine do indeed significantly reduce the cross-flow separation on the submarine in a high angle of incidence.

These methods mentioned above rely mainly on alterations of the submarine geometry, making it time- and money-consuming to rebuild or modify the models. Thus, it is desirable to find new methods to control the vortices with an easy, efficient and meaningful manner. Based on the Liutex vortex definition and identification system, Yu and Wang[19] explored the possibility of numerically manipulating vortices, and then deducted control strategies. Two methodologies, namely centripetal force field model and counter-rotation force field model respectively were proposed to be added in the control equations, which directly exerted in the vortex regions to modify the vortices. Wang et al.[20] applied the methods to flow past a cylinder at $Re = 200$ and a cavitating flow around Clark-Y hydrofoil with cavitation number of 0.8. Results showed that the models were effective ways to modify the flow field with purposes of controlling vortices. Zhao et al.[21] investigated the influence of the constructed Liutex force model on vortical structures. Flow past a cylinder at $Re = 100$ was numerically studied with different source terms with regard to magnitude and region. Results demonstrated that Liutex force field model could effectively strengthen or weaken the vortical structures based on different purpose. These researches have paved the way to numerically control and manipulate the flow field and vortices, but the application and test cases are all two-dimensional simple geometries at very low Reynolds number. In this article, we devote to extend the methods to three dimensional fully turbulent simulation of a submarine with various appendages.

The paper is outlined as follows. Firstly, the Liutex vortex identification and force field model are introduced. Then, the numerical simulation methods including computational domain, discretized mesh, turbulence modeling, initial and boundary conditions and solvers setup are given. Two simulations without and with Liutex force field model are conducted and compared with each other and experimental data. The resistance acting on the submarine, pressure and velocity flow field, as well as vortical structures are analyzed and compared sequentially. Lastly, the conclusions are drawn.

1. The Liutex force field model

1.1 *The Liutex vortex identification method*

Liu et al.[22] have been devoted to developing new vortex identification methods, including Omega, Liutex, and Omega-Liutex. According to the definition, Liutex is a vector defined as $\boldsymbol{R} = R\boldsymbol{r}$, where R is the magituede of Liutex, and $\boldsymbol{r}$ is the direction of Liutex[23]. This method removes vorticity due to shear motion and keeps the pure rotational motion part only, making it a powerful vortex identification and visualization tool for ship and marine hydrodynamics[24]. As explained by Xu et al.[25], $\boldsymbol{r}$ is the normalized real eigenvector of the vorticity gradient tensor such that $\boldsymbol{\omega} \cdot \boldsymbol{r} > 0$ and the explicit formula of R is

$$R = \boldsymbol{\omega} \cdot \boldsymbol{r} - \sqrt{(\boldsymbol{\omega} \cdot \boldsymbol{r})^2 - 4\lambda_{ci}^2} \tag{1}$$

where $\boldsymbol{\omega}$ is the vorticity vector, λ_{ci} is the imaginary part of the complex eigenvalue of the velocity gradient tensor. The Liutex method is classified as the third-generation vortex identification method, while the Q method, λ_{ci} criterion and λ_2 criterion are all classified as second generation methods since they are all scalar and eigenvalue

related. Liutex is a vector which overcomes the drawbacks of the scalar methods, e.g., it can give the direction of rotation and represents the rotational strength accurately.

1.2 *The Liutex force field model*

To achieve the purpose of flow control and vortex manipulation, an innovative method is proposed to modify the Navier-Stokes equations by adding an extra source term. The governing equations can be expressed as follows

$$\frac{\partial \boldsymbol{u}}{\partial t}+(\boldsymbol{u}\cdot\nabla)\boldsymbol{u}=-\nabla\frac{p}{\rho}+\nabla\cdot(\nu\nabla\boldsymbol{u})+c\boldsymbol{a} \tag{2}$$

where $\boldsymbol{u}$ is the velocity vector field, p, ρ and ν represent the pressure, density and kinematic viscosity of the fluid, respectively, c is a constant to control the magnitude or strength of the added force field, and $\boldsymbol{a}$ is the Liutex force field source term. The above formula describes the momentum equations for incompressible flow with Liutex force field model.

In the previous works[19-21], two Liutex force field models have been proposed. The first one is a centripetal model, which is expressed by

$$\boldsymbol{a}=\frac{\boldsymbol{R}}{2}\times\left(\frac{\boldsymbol{R}}{2}\times\boldsymbol{l}\right)=\frac{1}{4}\boldsymbol{R}\times(\boldsymbol{R}\times\boldsymbol{l}) \tag{3}$$

where $\boldsymbol{l}$ is a vector that starting at any field point P and ending at the local minimum pressure point P_0 which is regarded as the vortex core center point. $\boldsymbol{R}/2$ is half of the Liutex vector and represents the angular velocity of the rigid rotation part at P around vortex center core center P_0.

The second force field model that involves a time scale given by

$$\boldsymbol{a}=-\frac{1}{2\tau}(\boldsymbol{R}\times\boldsymbol{l}) \tag{4}$$

where the time scale τ acts like a relaxation time during which the rigid rotation of the fluid is ceased gradually and the velocity is decreased to zero.

The incompressible Navier-Stokes solver is modified to include the Liutex source term in the momentum equations. A two-step methodology is applied for the solving procedure. Firstly, the Liutex vector and corresponding centripetal acceleration vector are calculated at the current time step for each cell. Then, the modified Navier-Stokes equations with additional Liutex source term are solved to obtain the velocity and pressure field for the next time step.

2. Numerical methods

2.1 *DARPA Suboff geometry*

In this paper, a generic fully appended submarine model, DARPA Suboff AFF8 is chosen as the test case[26]. Figure 1 shows that the model consists of a bare hull, a sail with cap, and four control surfaces. Table 1 gives the principal parameters of the DARPA Suboff model.

Fig. 1 (Color online) The fully appended DARPA Suboff model

Table 1 Main particulars of the DARPA Suboff model

Item	Value
Length overall, L_{oa}	4.356 m
Length between perpendiculars, L_{pp}	4.261 m
Maximum hull diameter, $D_{\max}$	0.508 m
Center of buoyancy, LCB	$0.4621L_{oa}$
Volume of displacement, ∇	0.718 m^3
Wetted surface area, S	6.338 m^2

2.2 *Computational domain and mesh*

The overall dimensions of the computational domain are as follows: the inlet boundary is located at L_{oa} in front of the hull, whereas the outlet is located at $2L_{oa}$ behind the hull. Lateral frontiers are located L_{oa} on the far field boundaries. It is sketched schematically in Fig. 2. This configuration has been tested and used by several researches, and proved to be effective.

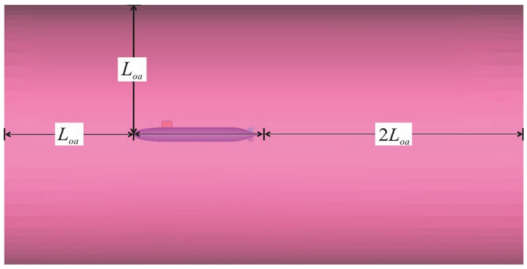

Fig. 2 (Color online) The computational domain configuration

A mesh presents the physical domain in a discrete form on which the governing equations can be resolved numerically. A high-quality mesh is essential to achieve converged and accurate results. Structured mesh has been proven to be more efficient and accurate. The multi-block based structured mesh

is built using the commercial software ICEM CFD. A very carefully designed O-grid topology is applied around the submarine model. The inner zone near the body, extending to the height of the sail outward distance is treated as a boundary layer refinement area, designed to capture the boundary layer and flow separation; the outer zone is used to provide a fine mesh density to resolve the flow field and offer a balance of resolution and computational cost. The total number of cells is 3 740 680. Details of the mesh is depicted in Fig. 3.

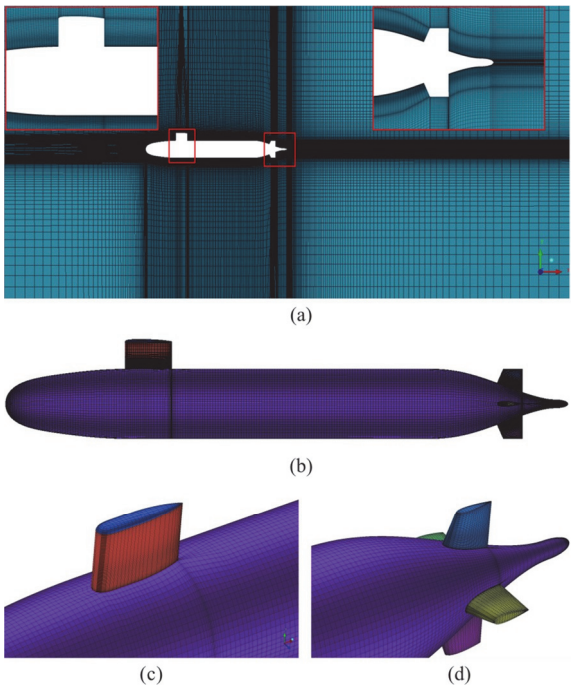

Fig. 3 Details of the mesh: (a) The longitudinal section in center plane, (b) Surface mesh of the hull, (c) Surface mesh of sail and sail cap, (d) Surface mesh of tail and fins

2.3 *Turbulence modeling*

Reynolds averaged Navier-Stokes (RANS) equations are suitable for engineering applications, and typically offer the level of accuracy required and provide the most economical approach. In this paper, the shear stress transport (SST) $k-\omega$ model with low y^+ wall treatment method is utilized[3]. The turbulence kinetic energy k and specific dissipation rate ω transport equations of SST k-ω turbulence model are as follows:

$$\frac{\partial(\rho k)}{\partial t}+\frac{\partial(\rho k u_i)}{\partial x_j}=\frac{\partial}{\partial x_j}\left[\left(\mu+\frac{\mu_t}{\sigma_k}\right)\frac{\partial k}{\partial x_j}\right]+P_k-D_k+S_k \tag{5}$$

$$\frac{\partial(\rho\omega)}{\partial t}+\frac{\partial(\rho\omega u_i)}{\partial x_j}=\frac{\partial}{\partial x_j}\left[\left(\mu+\frac{\mu_t}{\sigma_\omega}\right)\frac{\partial\omega}{\partial x_j}\right]+P_\omega-D_\omega+CD_\omega+S_\omega \tag{6}$$

where σ_k and σ_ω are the turbulent Prandtl numbers for k and ω, P_k and P_ω are the productions of k and ω, respectively, D_k and D_ω are the dissipations of k and ω, respectively, CD_ω denotes the Cross- Diffusion term, S_k and S_ω are the user-defined terms.

2.4 *Boundary and initial conditions*

There are four boundary conditions utilized in the simulation. As depicted in Fig. 2, the upstream is treated as velocity inlet boundary on which velocity magnitude U based on Re is imposed. The downstream boundary is specified to be pressure outlet, and the far field boundary is treated as symmetric plane. No-slip condition is specified for the submarine hull.

The simulations in this paper are performed with the open source code OpenFOAM. It is a free and powerful solution for solving multidisciplinary problems in fluid dynamics. The solver uses a cell-centred finite volume discretization applied to cells of arbitrary polyhedral cells, and offers a selection of turbulence models suitable for a wide range of practical applications. The computational matrix for the simulations is listed in Table 2. Two simulations that $Re=1.2\times10^7$, while Liutex force field model activated or not are performed, respectively.

Table 2 Computational matrix

Cases	1	2
Re	1.2×10^7	1.2×10^7
Liutex force field model	Deactivated	Activated

3. Results and discussion

3.1 *Resistance force*

Figure 4 presents the resistance computations as a function of advance speeds. The present computational values are compared against the experimental data measured in a deep water towing tank and numerical results from Chase[26], who predicted the resistance by RANS and Delayed DES (DDES) computations. The present result without Liutex force field model shows great consistency to the experimental values. However, it is interesting to find that the resistance with Liutex force field model is reduced by 9.31%, which means that the Liutex force field model do indeed change the flow field.

3.2 *Pressure and velocity distribution*

To reveal the reason of resistance decrease, pressure and velocity flow fields are derived and

analyzed. Figure 5 shows the surface distribution of pressure for both cases without/with Liutex force field model. The main characteristics include the stagnation points located at the nose, the middle lines of sail and control surfaces, where the pressure reaches the maximum. As for the two cases, almost no difference is observed. Figure 6 demonstrates the axial velocity (u/U) contour on the longitudinal middle plane. Obvious differences can be seen in the velocity flow field, especially in the local regions just behind the appendages, where axial velocity is apparently decreased. According to the Bernoulli's principle, lower velocity will cause higher pressure, thus making the pressure differences between the back and forth smaller, which results in a resistance decrease.

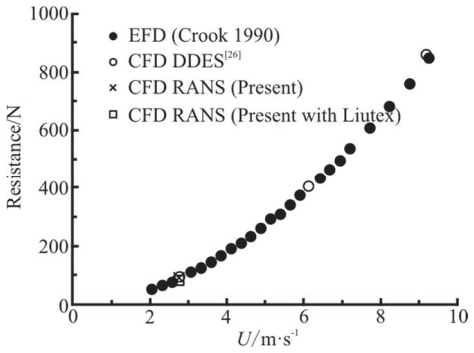

Fig. 4 Comparison of resistance at different speeds

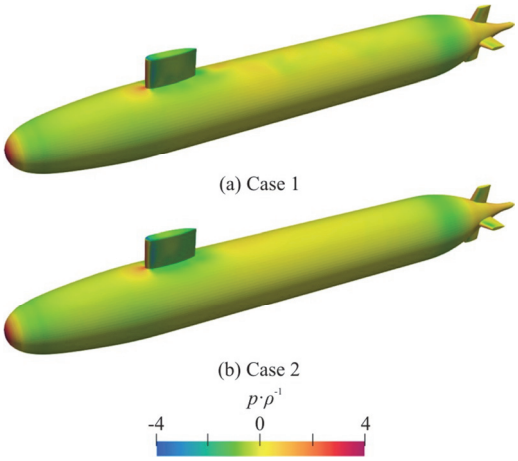

Fig. 5 (Color online) Surface pressure distribution of both cases

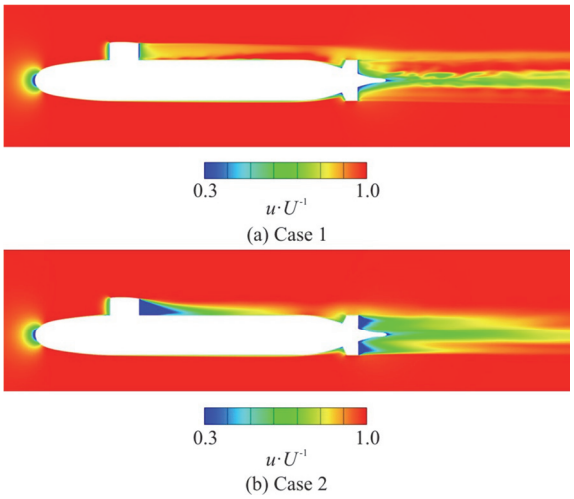

Fig. 6 (Color online) Axial velocity contour on the longitudinal middle plane of both cases

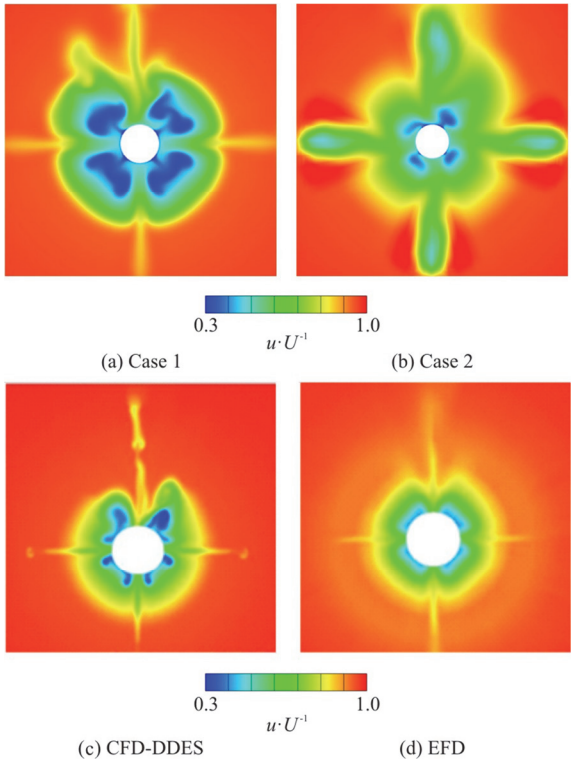

Fig. 7 (Color online) Wake comparison at $x/L_{oa} = 0.987$

Figure 7 shows the comparison of present numerical results with experimental and another numerical results available in the literature by wake profiles at the propeller plane behind the submarine hull. At this longitudinal location $x/L_{oa} = 0.987$, averaged velocity distribution in the axial direction is usually used to derive the nominal wake coefficient. In the picture, a V-shaped high-speed carving is observed on the sail side along the center plane. The clover-shaped pattern is explained to be due to the interaction of fins horseshoe vortices with the boundary layer, which pushes high momentum fluid behind the fins. All the calculations except case 2 predict the clover-shaped pattern and the V-shaped carving. Both the simulations present and Chase[26] predict a larger velocity deficit compared with the experiment in the clover

shape region. It also should be noted that in all the simulations the sail wake is tilted towards the right or left, which is due to an asymmetry in the sail tip vortex predictions. As for the case 2, in which Liutex force field model plays an important role in the development of flow field, the overall pattern of wake is totally different. The clover-shaped pattern in the boundary layer is much smaller, while the V-shaped carving is replaced by an opposite hump. A cruciform flow structure induced by four fins can be seen clearly. It can be concluded that the appendages affect the velocity distribution significantly on the propeller plane. Although the mechanism is to be explored further, the differences between cases 1 and 2 demonstrate the great impact of Liutex force field model on flow control.

Figure 8 depicts axial velocity contours along the hull in 15 uniformly distributed cut planes (x/L_{oa} = 0.1, 0.2, 0.3, 0.4, 0.5, 0.6, 0.7, 0.8, 0.9, 1.0, 1.1, 1.2, 1.3, 1.4 and 1.5). The flow pattern at different sections of the hull provides details of flow development over the hull length. For case 1, the wake development details can be observed as the boundary layer gets thinner immediately downstream of the sail and thicker on the sides of this depleted area. The contours behind the fins show a clover-shaped large velocity deficit in the boundary layer between the fins, deficits behind the fins, and a deficit above the sail (on the sail side) due to the sail wake, as illustrated in Fig. 7. Notice that the high velocity observed in the wake of the sail, where necklace vortices deplete the boundary layer at the center and send low momentum flow to the sides, causing a V-shaped high-speed carving in the wake. Far away in the downstream direction from the hull, the effect on the velocity values due to appendages are decreasing and finally it becomes almost equal to the freestream velocity. While for case 2, there are remarkable differences in the shapes of the contours, which are much thicker and fatter than case 1. The tuning effect of Liutex force field model results in a significantly different wake pattern.

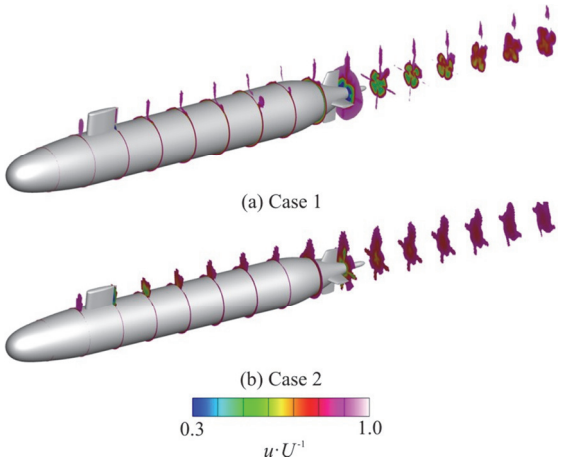

Fig. 8 (Color online) Axial velocity contours at uniformly distributed sections at x/L_{oa} = 0.1, 0.2, 0.3, 0.4, 0.5, 0.6, 0.7, 0.8, 0.9, 1.0, 1.1, 1.2, 1.3, 1.4 and 1.5

3.3 *Coherent vortical structures*

The three-dimensional visualization of vortical structures can be expressed by Q-criterion which defines a vortex by the region where the rate of rotation tensor Ω_{ij} exceeds strain rate tensor S_{ij} [27].

$$Q = \frac{1}{2}(|\Omega|^2 - |S|^2), \quad \Omega_{ij} = \frac{1}{2}\left(\frac{\partial u_i}{\partial x_j} - \frac{\partial u_j}{\partial x_i}\right),$$

$$S_{ij} = \frac{1}{2}\left(\frac{\partial u_i}{\partial x_j} + \frac{\partial u_j}{\partial x_i}\right) \tag{7}$$

As shown in Fig. 9, the iso-surface of $Q=10$ for both cases are provided. The simulations predict the main features, i.e., sail horseshoe vortex, sail wake, sail tip vortex pair, and horseshoe, wake and tip vortices from the fins. However, the strength and extent of the vortices, including their breakup, varies a lot depending on the Liutex force field model used or not. The case 2 shows huge asymmetry in the sail tip vortex pair, and these vortices intertwine with each other when propagate downstream. The tip vortices of the sail and fins in case 2 are twisted and discharged into the wakes, results in a bunch of vortex tubes with bigger diameter than case 1. The sail tip vortices in case 1 extend a long distance to almost the fins location, but the sail horseshoe vortex dissipates quickly by $x/L_{oa} = 0.4$. The introduction of Liutex force field model greatly changes the vortical structures of the submarine, which undoubtedly will have a potential use for flow control and vortex manipulation.

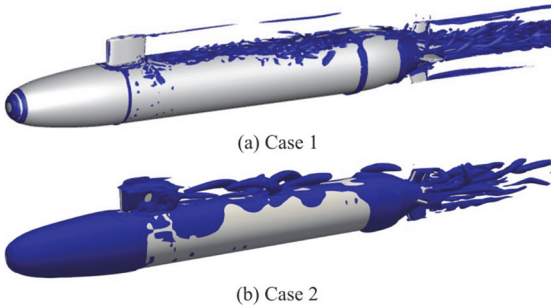

Fig. 9 (Color online) Iso-surface of $Q=10$ for both cases

4. Conclusion

The present work is devoted to a preliminary research on vortex tuning of a three-dimensional fully appended submarine at high Reynolds number by using Liutex force field model. An extra source term derived from the Liutex vector is added to the Navier-Stokes equations. Results demonstrate that Liutex force field model has a great impact on the resistance acting on the submarine, pressure and velocity distribution, as well as the vortical structures. The resistance of the hull with Liutex force field model has reduced by 9.31%, and the flow field is totally different with that of common condition. This paper has established an initial step towards the goal of flow control and vortex manipulation based on the Liutex force field model for ship hydrodynamics. Further efforts can be devoted to exploring the mechanisms and potential use in industrial and practical applications.

Acknowledgement

This work was supported by the Oceanic Interdisciplinary Program of Shanghai Jiao Tong University (Grant No. SL2020PT104).

References

[1] Ashok A., Van B. T., Smits A. J. The structure of the wake generated by a submarine model in yaw [J]. *Experiments in Fluids*, 2015, 56(6): 123.

[2] Martin J. E., Michael T., Carrica P. M. Submarine maneuvers using direct overset simulation of appendages and propeller and coupled CFD/potential flow propeller solver [J]. *Journal of Ship Research*, 2015, 59(1): 31-48.

[3] Phillips A. B., Turnock S. R., Furlong M. Influence of turbulence closure models on the vortical flow field around a submarine body undergoing steady drift [J]. *Journal of Marine Science and Technology*, 2010, 15(3): 201-217.

[4] Jimenez J. M., Hultmark M., Smits A. J. The intermediate wake of a body of revolution at high Reynolds numbers [J]. *Journal of Fluid Mechanics*, 2010, 659: 516-539.

[5] Ashok A., Van B. T., Smits A. J. Asymmetries in the wake of a submarine model in pitch [J]. *Journal of Fluid Mechanics*, 2015, 774: 416-442.

[6] Shariati S. K., Mousavizadegan S. H. The effect of appendages on the hydrodynamic characteristics of an underwater vehicle near the free surface [J]. *Applied Ocean Research*, 2017, 67: 31-43.

[7] Doyle R., Jeans T. L., Holloway A. G. L., et al. URANS simulations of an axisymmetric submarine hull undergoing dynamic sway [J]. *Ocean Engineering*, 2019, 172: 155-169.

[8] Posa A., Balaras E. A numerical investigation about the effects of Reynolds number on the flow around an appended axisymmetric body of revolution [J]. *Journal of Fluid Mechanics*, 2020, 884: A41.

[9] Posa A., Balaras E. Large-eddy simulations of a notional submarine in towed and self-propelled configurations [J]. *Computers and Fluids*, 2018, 165: 116-126.

[10] Fureby C., Anderson B., Clarke D. et al. Experimental and numerical study of a generic conventional submarine at 10° yaw [J]. *Ocean Engineering*, 2016, 116: 1-20.

[11] Dubbioso G., Broglia R., Zaghi S. CFD analysis of turning abilities of a submarine model [J]. *Ocean engineering*, 2017, 129: 459-479.

[12] Chase N., Michael T., Carrica P. M. Overset simulation of a submarine and propeller in towed, self-propelled and maneuvering conditions [J]. *International Shipbuilding Progress*, 2013, 60(1-4): 171-205.

[13] Liu Z. H., Xiong Y., Wang Z. Z. et al. Numerical simulation and experimental study of the new method of horseshoe vortex control [J]. *Journal of Hydrodynamics*, 2010, 22(4): 572-581.

[14] Liu Z., Xiong Y., Tu C. Method to control unsteady force of submarine propeller based on the control of horseshoe vortex [J]. *Journal of Ship Research*, 2012, 56(1): 12-22.

[15] Liu Z. H., Xiong Y., Tu C. X. The method to control the submarine horseshoe vortex by breaking the vortex core [J]. *Journal of Hydrodynamics*, 2014, 26(4): 637-645.

[16] Liu Y., Li Y., Shang D. The hydrodynamic noise suppression of a scaled submarine model by leading-edge serrations [J]. *Journal of Marine Science and Engineering*, 2019, 7(3): 68.

[17] Saeidinezhad A., Dehghan A. A., Dehghan M. M. Nose shape effect on the visualized flow field around an axisymmetric body of revolution at incidence [J]. *Journal of Visualization*, 2015, 18(1): 83-93.

[18] Manshadi M. D., Hejranfar K., Farajollahi A. H. Effect of vortex generators on hydrodynamic behavior of an underwater axisymmetric hull at high angles of attack [J]. *Journal of Visualization*, 2017, 20(3): 559-579.

[19] Yu H. D., Wang Y. Q. Liutex-based vortex dynamics: A preliminary study [J]. *Journal of Hydrodynamics*, 2020, 32(6): 1217-1220.

[20] Wang Y. Q., Yu H. D., Zhao W. W. et al. Liutex-based vortex control with implications for cavitation suppression [J]. *Journal of Hydrodynamics*, 2021, 33(1): 74-85.

[21] Zhao W. W., Wang Y. Q., Chen S. T. et al. Parametric study of Liutex-based force field models [J]. *Journal of Hydrodynamics*, 2021, 33(1): 86-92.

[22] Liu C., Gao Y., Tian S., et al. Rortex–A new vortex vector definition and vorticity tensor and vector decompositions [J]. *Physics of Fluids*, 2018, 30(3): 35103.

[23] Wang Y. Q., Gao Y. S., Xu H. et al. Liutex theoretical system and six core elements of vortex identification [J]. *Journal of Hydrodynamics*, 2020, 32(2): 197-211.

[24] Zhao W. W., Wang J. H., Wan D. C. Vortex identification methods in marine hydrodynamics [J]. *Journal of Hydrodynamics,* 2020, 32(2): 286-295.

[25] Xu W., Gao Y., Deng Y. et al. An explicit expression for the calculation of the Rortex vector [J]. *Physics of Fluids*, 2019, 31(9): 95102.

[26] Chase N. Simulations of the DARPA Suboff submarine including self-propulsion with the E1619 propeller [D]. Master Thesis, Iowa City, USA: University of Iowa, 2012.

[27] Cao L. S., Huang F. L., Liu C. et al. Vortical structures and wakes of a sphere in homogeneous and density stratified fluid [J]. *Journal of Hydrodynamics*, 2021, 33(2): 207-215.